Mixed-valence correlations in charge-transferring atom–surface collisions

2015 Phys. Scr. 2015 014008

(http://iopscience.iop.org/1402-4896/2015/T165/014008)

IOP Publishing | Royal Swedish Academy of Sciences Physica Scripta

Phys. Scr. **T165** (2015) 014008 (9pp) doi:10.1088/0031-8949/2015/T165/014008

Mixed-valence correlations in charge-transferring atom–surface collisions

M Pamperin, F X Bronold and H Fehske

Institut für Physik, Ernst-Moritz-Arndt-Universität Greifswald, D-17489 Greifswald, Germany

Received 29 March 2014
Accepted for publication 21 November 2014
Published 7 October 2015

Abstract

Motivated by experimental evidence (He and Yarmoff 2010 *Phys. Rev. Lett.* **105** 176806) for a mixed-valence state to occur in the neutralization of strontium ions on gold surfaces we analyze this type of charge-transferring atom–surface collision from a many-body theoretical point of view using quantum-kinetic equations together with a pseudo-particle representation for the electronic configurations of the atomic projectile. Particular attention is paid to the temperature dependence of the neutralization probability which—experimentally—seems to signal mixed-valence-type correlations affecting the charge-transfer between the gold surface and the strontium projectile. We also investigate the neutralization of magnesium ions on a gold surface which shows no evidence for a mixed-valence state. Whereas for magnesium excellent agreement between theory and experiment could be obtained, for strontium we could not reproduce the experimental data. Our results indicate mixed-valence correlations to be in principle present, but for the model mimicking most closely the experimental situation they are not strong enough to affect the neutralization process quantitatively.

Keywords: mixed-valence correlations, charge-transfer, atom–surface collision

(Some figures may appear in colour only in the online journal)

1. Introduction

Charge-exchange between an atomic projectile and a surface plays a central role in surface science [1–6]. Many surface diagnostics, for instance, secondary ion mass spectrometry [7] or meta-stable atom de-excitation spectroscopy [8] utilize surface-based charge-transfer processes. The same holds for plasma science. Surface-based production of negative hydrogen ions, for instance, is currently considered as a pre-stage process in neutral gas heating of fusion plasmas [9]. The operation modii of low-temperature gas discharges [10], which are main work horses in many surface modification and semiconductor industries, depend on secondary electron emission from the plasma walls and thus also on surface-based charge-transfer processes.

Besides their great technological importance, charge-transferring atom–surface collisions are however also of fundamental interest. This type of collision couples a local quantum system with a finite number of discrete states—the projectile—to a large reservoir with a continuum of states—the target. Irrespective of the coupling between the two, either due to tunneling or due to Auger-type Coulomb interaction, charge-transferring atom–surface collisions are thus perfect realizations of time-dependent quantum impurity systems [11, 12]. By a judicious choice of the projectile-target combination as well as the collision parameters Kondo-type features [13] are thus expected as in any other quantum impurity system [14–17].

Indeed a recent experiment by He and Yarmoff [18, 19] provides strong evidence for electron correlations affecting the neutralization of positively charged strontium ions on gold surfaces. The fingerprint of correlations could be the experimentally found negative temperature dependence of the neutralization probability. It may arise [11, 12] from thermally excited conduction band holes occupying the strongly renormalized $5s^1$ configuration of the projectile which effectively stabilizes the impinging ion and reduces thereby the neutralization probability. The purpose of the present work is to analyze the He–Yarmoff experiment [18, 19] from a genuine many-body theoretical point of view, following the seminal work of Nordlander and coworkers [11, 20–23] as well as Merino and Marston [12] and to provide theoretical support for the interpretation of the experiment in terms of a mixed-valence scenario.

We couch—as usual—the theoretical description of the charge-transferring atom–surface collision in a time-dependent Anderson impurity model [3–6, 24–30]. The parameters of the model are critical. To be as realistic as possible without performing an expensive *ab initio* analysis of the ion–surface interaction we employ for the calculation of the model parameters Gadzuk's semi-empirical approach [31, 32] based on image charges and Hartree–Fock wave functions for the projectile states [33]. The time-dependent Anderson model, written in terms of pseudo-operators [34, 35] for the projectile states, is then subjected to a full quantum-kinetic analysis using contour-ordered Green functions [36, 37] and a non-crossing approximation for the hybridization self-energies as originally proposed by Nordlander and coworkers [11, 20–23].

We apply the formalism to analyze, respectively, the neutralization of a strontium and a magnesium ion on a gold surface. For the Mg:Au system, which shows no evidence for mixed-valence correlations affecting the charge-transfer between the surface and the projectile, we find excellent agreement between theory and experiment. For the Sr:Au system, in contrast, we could reproduce only the correct order of magnitude of the neutralization probability. Its temperature dependence could not be reproduced. Our modeling shows however that a mixed-valence scenario could in principle be at work. For the material parameters best suited for the description of the Sr:Au system they are however not strong enough to affect the neutralization probability also quantitatively.

The outline of our presentation is as follows. In the next section we describe the time-dependent Anderson model explaining in particular how we obtained the parameters characterizing it. Section 3 concerns the quantum kinetics and presents the set of coupled two-time integro-differential equations which have to be solved for determining the probabilities with which the various charge states of the projectile occur. They form the basis for the analysis of the temperature dependence of the neutralization probability. Numerical results for a strontium as well as a magnesium ion hitting a gold surface are presented, discussed, and compared to experimental data in section 4. Concluding remarks are given in section 5.

2. Model

When an atomic projectile approaches a surface its energy levels shift and broaden due to direct and exchange Coulomb interactions with the surface. Since the target and the projectile are composite objects the calculation of these shifts and broadenings from first principles is a complicated problem [38]. We follow therefore Gadzuk's semi-empirical approach [31, 32]. From our previous work on secondary electron emission due to de-excitation of meta-stable nitrogen molecules on metal [39] and dielectric [40, 41] surfaces we expect the approach to give reasonable estimates for the level widths as well as the level positions for distances from the surface larger than a few Bohr radii. In addition, the approach has a clear physical picture behind it and is thus intuitively very appealing.

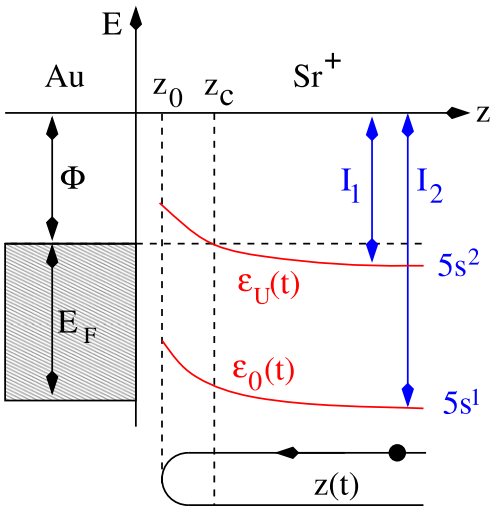

Figure 1. Illustration of the time-dependent quantum impurity model used for the description of the charge-transferring scattering of a Sr^+ ion on a gold surface. The two ionization energies, $\varepsilon_U(t)$ and $\varepsilon_0(t)$, standing for the projectiles' $5s^2$ and $5s^1$ configuration, respectively, shift due to the image interaction with the surface. Far away from the surface the two energies merge, respectively, with the first (I_1) and the second (I_2) ionization energy of a strontium atom. The image interaction also leads to a hybridization of the Sr states with the conduction band states of the surface which is characterized by a step potential at $z = 0$ whose depth is the sum of the work function $\Phi > 0$ and the Fermi energy $E_F > 0$. For simplicity the broadening is not shown. Indicated however is the trajectory $z(t)$ of the ion. Important points along the trajectory are z_0, the turning point, and z_c, the point where the first ionization level crosses the Fermi energy.

The essence of the model is illustrated in figure 1. It shows for the particular case of a strontium ion hitting a gold surface the energy levels of the projectile closest to the Fermi energy of the target. Quite generally, for alkaline-earth (AE) ions the first and the second ionization levels are most important. Identifying the positive ion (AE^+) with a singly occupied impurity and the neutral atom (AE^0) with a doubly occupied impurity, the projectile can be modelled as a non-degenerate, asymmetric Anderson model with on-site energies

$$\varepsilon_U(z) = -I_1 + \frac{e^2}{4|z - z_i|}, \tag{1}$$

$$\varepsilon_0(z) = -I_2 + \frac{3e^2}{4|z - z_i|}, \tag{2}$$

where $I_1 > 0$ and $I_2 > 0$ are, respectively, the first and second ionization energy far away from the surface while z_i is the distance of the metal's image plane from its crystallographic ending at $z = 0$. The on-site Coulomb repulsion $U(z)$ would be the difference of the two energies. Table 1 summarizes the material parameters required for the modeling of the neutralization of strontium and magnesium ions on a gold surface.

Table 1. Material parameters for magnesium, strontium and gold: I_1 and I_2 are the first and the second ionization energy, Z_1 and Z_2 are the effective charges to be used in the calculation of the hybridization matrix element (viz: equation (9)), Φ is the work function, E_F the Fermi energy, z_i the position of the image plane in front of the surface, and m_e^* is the effective mass of an electron.

	I_1(eV)	Z_1	I_2(eV)	Z_2	Φ(eV)	E_F(eV)	z_i(a.u.)	m_e^*/m_e
Sr	5.7	1.65	11.0	2	–	–	–	–
Mg	7.65	1.65	15.04	2	–	–	–	–
Au	–	–	–	–	5.1–5.2	5.53	1.0	1.1

The z-dependent shifts of the ionization levels can be obtained as the energy gain of a virtual process moving the configuration under consideration from the actual position z to $z = \infty$, reducing its electron occupancy by one, and then moving it back to position z, taking into account in both moves—if present—image interactions due to the charge state of the final and initial configurations with the metal [42]. For the upper level, ε_U, that is, the $5s^2$ configuration the cycle is $AE \rightarrow AE^+ + e^- \rightarrow AE^+$, whereas for the lower level, ε_0, that is, the $5s^1$ configuration the cycle is $AE^+ \rightarrow AE^{2+} + e^- \rightarrow AE^{2+}$.

To set up the Hamiltonian we also need the wave functions for the projectile states. For the upper level we use the (ns) Hartree–Fock wave function of an AE atom while for the lower level we use the (ns) Hartree–Fock wave function of an AE^+ ion. According to Clementi and Roetti [33] both can be written in the form

$$\psi_{HF}(\vec{r}) = Y_{00}(\theta, \phi) \sum_{j=1}^{N} c_j N_j \, |\vec{r}|^{n_j - 1} e^{-C_j |\vec{r}|} \tag{3}$$

with c_j, n_j, C_j, and N_j tabulated parameters and $Y_{00}(\theta, \phi)$ the spherical harmonics with $m = l = 0$.

For simplicity we assume the projectile to approach the surface from $z = \infty$ on a perpendicular trajectory

$$z(t) = z_0 + v|t|, \tag{4}$$

with the turning point z_0 reached at time $t = 0$ and v the velocity of the projectile. The lateral motion of the projectile is thus ignored. To be consistent with this simple trajectory we also neglect the lateral variation of the potential characterizing the metal surface. The electrons of the metal are thus simply described in terms of a potential step at $z = 0$ with depth $-|V_0| = \Phi + E_F$, where $\Phi > 0$ is the work function of the metal and $E_F > 0$ is its Fermi energy measured from the bottom of the conduction band (see table 1), leading to

$$\varepsilon_{\vec{k}} = \frac{\hbar^2}{2m_e^*}\left(k_x^2 + k_y^2 + k_z^2\right) - |V_0|, \tag{5}$$

$$\psi_{\vec{k}}(\vec{r}) = \frac{1}{L\sqrt{L}} e^{i(k_x x + k_y y)} \Big\{ T_{k_z} e^{-\kappa_{k_z} z} \Theta(z) + \left[e^{ik_z z} + R_{k_z} e^{-ik_z z} \right] \Theta(-z) \Big\}, \tag{6}$$

for the energies and wave functions of the conduction band electrons; L is the spatial width of the step (drops out in the final expressions) and

$$R_{k_z} = \frac{ik_z + \kappa_{k_z}}{ik_z - \kappa_{k_z}}, \tag{7}$$

$$T_{k_z} = \frac{2ik_z}{ik_z - \kappa_{k_z}}, \tag{8}$$

with $\kappa_{k_z} = \sqrt{2m_e^*(|V_0| - k_z^2)/\hbar^2}$ are the reflection and transmission coefficients of the potential step.

While the projectile is on its trajectory its ionization levels hybridize with the conduction band. The matrix element for this process is given by [31, 32]

$$V_{\vec{k}}(t) = \int_{z>0} d^3r \, \psi_{\vec{k}}^*(\vec{r}) \frac{Ze^2}{|\vec{r} - \vec{r}_p(t)|} \psi_{HF}(\vec{r} - \vec{r}_p(t)), \tag{9}$$

where the potential between the two wave functions is the residual Coulomb interaction of the valence electron with the core of the projectile located at $\vec{r}_p(t) = z(t)\vec{e}_z$. The matrix element can be transformed to a level width

$$\Gamma_{\varepsilon(t)}(t) = 2\pi \sum_{\vec{k}} |V_{\vec{k}}(t)|^2 \, \delta(\varepsilon(t) - \varepsilon_{\vec{k}}) \tag{10}$$

which is an important quantity. The charge Z in equation (9) is the charge of the nucleus screened by all the electrons of the projectile except of the valence electron under consideration. For the hybridization of the lower level, the second ionization level, $Z = 2$ while for the hybridization of the upper level, the first ionization level, $Z = 2 - s$, where $s = 0.35$ is

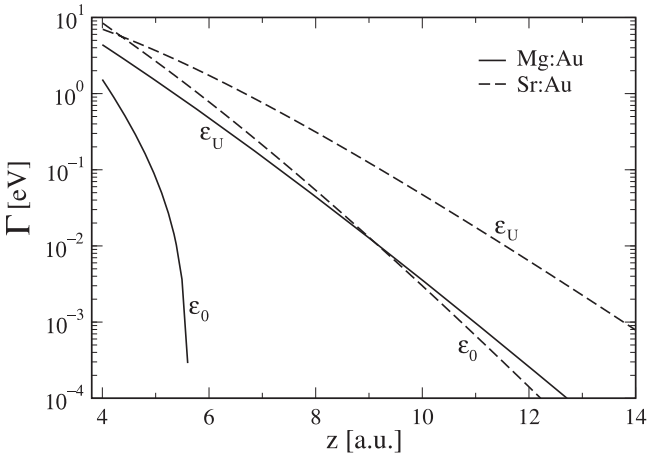

Figure 2. Level widths as obtained from equation (10) for the Mg:Au (solid lines) and the Sr:Au (dashed lines) system.

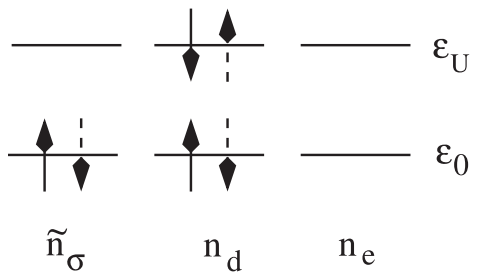

Figure 3. Possible configurations of the AE projectile. Solid and dashed arrows indicate, respectively, spin-reversed states which are energetically degenerate. The quantities $\tilde{n}_\sigma$, n_d, and n_e are, respectively, the (pseudo) probabilities with which the AE^+, the AE^0, and the AE^{2+} configuration occur.

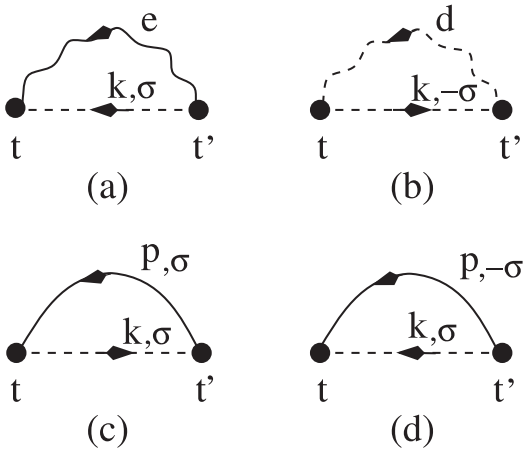

Figure 4. Self-energies in the non-crossing approximation. Straight dashed lines denote bare Green functions for the conduction band electrons. The other lines indicate renormalized Green functions for the singly occupied (p), the empty (e), and the doubly occupied (d) AE projectile. Filled bullets stand for the hybridization matrix element $V_{\vec{k}}(t)$. Diagrams (a) and (b) give, respectively, the self-energies $\Sigma_{0,\sigma}$ and $\Sigma_{U,\sigma}$ for the Green function P_σ. The self-energies Π_e and Π_d for the Green functions E and D, respectively, are shown in (c) and (d).

Slater's shielding constant due to the second electron in the s-valence shell [43].

In figure 2 we show the level widths calculated from equation (10) with $\varepsilon(t)$ set, respectively, to $\varepsilon_U(t)$ and $\varepsilon_0(t)$, for magnesium and strontium using the parameters of table 1. Most probably we overestimate the widths close to the surface. To what extent, however, only precise calculations of the kind performed for alkaline ions by Nordlander and Tully can show [38].

Using Coleman's pseudo-particle representation [34, 35] for the projectile configurations illustrated in figure 3, the Hamiltonian describing the interaction of an AE projectile with a metal surface can be written as [23]

$$\begin{aligned} H(t) = &\sum_\sigma \varepsilon_0(t) p_\sigma^\dagger p_\sigma^\dagger + \left[\varepsilon_0(t) + \varepsilon_U(t)\right] d^\dagger d^\dagger \\ &+ \sum_{\vec{k}\sigma} \varepsilon_{\vec{k}} c_{\vec{k}\sigma}^\dagger c_{\vec{k}\sigma}^\dagger + \sum_{\vec{k}\sigma}\left[V_{\vec{k}}(t) c_{\vec{k}\sigma}^\dagger e^\dagger p_\sigma^\dagger + \text{h. c.}\right] \\ &+ \sum_{\vec{k}\sigma}\left[V_{\vec{k}}(t) c_{\vec{k}\sigma}^\dagger d^\dagger p_{-\sigma}^\dagger + \text{h. c.}\right] \end{aligned} \tag{11}$$

with $e^\dagger$, $d^\dagger$, and $p_\sigma^\dagger$ denoting, respectively, the creation operators for an empty (AE^{2+}), a doubly occupied (AE^0), and a singly occupied (AE^+) projectile. Since the projectile can be only in either one of these configurations, the Hamiltonian has to be constrained by [34, 35]

$$Q = \sum_\sigma p_\sigma^\dagger p_\sigma^\dagger + d^\dagger d^\dagger + e^\dagger e^\dagger = 1. \tag{12}$$

This completes the description of the model. Combined with measured projectile velocities the model describes the charge-transfer responsible for the neutralization of AE ions on noble metal surfaces.

3. Quantum kinetics

To calculate the neutralization probability for the AE ion hitting the metal surface we follow Nordlander and coworkers [11, 20–23] and set up quantum-kinetic equations for contour-ordered Green functions [36, 37] describing the empty, singly, and doubly occupied projectile. We denote these functions, respectively, by $E(t, t')$, $P_\sigma(t, t')$, and $D(t, t')$ and write their analytic pieces in the form

$$\begin{aligned} H^{\mathrm{R}}(t, t') = &-\mathrm{i}\Theta(t - t') \\ &\times \exp\left[-\mathrm{i}\int_{t'}^{t} \mathrm{d}\bar{t}\,\varepsilon(\bar{t})\right] \bar{H}^{\mathrm{R}}(t, t'), \end{aligned} \tag{13}$$

$$H^{\gtrless}(t, t') = \exp\left[-\mathrm{i}\int_{t'}^{t} \mathrm{d}\bar{t}\,\varepsilon(\bar{t})\right] \bar{H}^{\gtrless}(t, t'), \tag{14}$$

where $H(t, t')$ can be any of the three Green functions and $\varepsilon(t)$ is, depending on the Green function, either identically 0, $\varepsilon_0(t)$, or $\varepsilon_0(t) + \epsilon_U(t)$.

Using this notation and calculating the self-energies Π_e, $\Sigma_{0,\sigma}$, $\Sigma_{U,\sigma}$, and Π_d in the non-crossing approximation diagrammatically shown in figure 4 leads after application of the Langreth–Wilkins rules [44] and the projection to the $Q = 1$ subspace [16, 20] to [22, 23]

$$\frac{\partial}{\partial t}\bar{E}^{\mathrm{R}}(t, t') = -\sum_\sigma \int_{t'}^{t} \mathrm{d}\bar{t}\,\bar{K}_{\varepsilon_0}^{<}(\bar{t}, t)\bar{P}_\sigma^{\mathrm{R}}(t, \bar{t})\bar{E}^{\mathrm{R}}(\bar{t}, t'), \tag{15}$$

$$\begin{aligned} \frac{\partial}{\partial t}\bar{P}_\sigma^{\mathrm{R}}(t, t') = &-\int_{t'}^{t} \mathrm{d}\bar{t}\,\bar{K}_{\varepsilon_0}^{>}(t, \bar{t})\bar{E}^{\mathrm{R}}(t, \bar{t})\bar{P}_\sigma^{\mathrm{R}}(\bar{t}, t') \\ &- \int_{t'}^{t} \mathrm{d}\bar{t}\,\bar{K}_{\varepsilon_U}^{<}(\bar{t}, t)\bar{D}^{\mathrm{R}}(t, \bar{t})\bar{P}_\sigma^{\mathrm{R}}(\bar{t}, t'), \end{aligned} \tag{16}$$

$$\frac{\partial}{\partial t}\bar{D}^{\mathrm{R}}(t, t') = -\sum_\sigma \int_{t'}^{t} \mathrm{d}\bar{t}\,\bar{K}_{\varepsilon_U}^{>}(t, \bar{t})\bar{P}_{-\sigma}^{\mathrm{R}}(t, \bar{t})\bar{D}^{\mathrm{R}}(\bar{t}, t'), \tag{17}$$

and

$$\frac{\partial}{\partial t}\bar{E}^{<}(t,t') = \sum_{\sigma}\int_{-\infty}^{t'} \mathrm{d}\bar{t}\,\bar{K}^{>}_{\varepsilon_0}(\bar{t},t)\bar{P}^{<}_{\sigma}(t,\bar{t})\left[\bar{E}^{\mathrm{R}}(t',\bar{t})\right]^{*} - \sum_{\sigma}\int_{-\infty}^{t} \mathrm{d}\bar{t}\,\bar{K}^{<}_{\varepsilon_0}(\bar{t},t)\bar{P}^{\mathrm{R}}_{\sigma}(t,\bar{t})\bar{E}^{<}(\bar{t},t'), \tag{18}$$

$$\begin{aligned}\frac{\partial}{\partial t}\bar{P}^{<}_{\sigma}(t,t') = {} & \int_{-\infty}^{t'} \mathrm{d}\bar{t}\,\bar{K}^{<}_{\varepsilon_0}(t,\bar{t})\bar{E}^{<}(t,\bar{t})\left[\bar{P}^{\mathrm{R}}_{\sigma}(t',\bar{t})\right]^{*} \\ & + \int_{-\infty}^{t'} \mathrm{d}\bar{t}\,\bar{K}^{>}_{\varepsilon_U}(\bar{t},t)\bar{D}^{<}(t,\bar{t})\left[\bar{P}^{\mathrm{R}}_{\sigma}(t',\bar{t})\right]^{*} \\ & - \int_{-\infty}^{t} \mathrm{d}\bar{t}\,\bar{K}^{>}_{\varepsilon_0}(t,\bar{t})\bar{E}^{\mathrm{R}}(t,\bar{t})\bar{P}^{<}_{\sigma}(\bar{t},t') \\ & - \int_{-\infty}^{t} \mathrm{d}\bar{t}\,\bar{K}^{<}_{\varepsilon_U}(\bar{t},t)\bar{D}^{\mathrm{R}}(t,\bar{t})\bar{P}^{<}_{\sigma}(\bar{t},t'),\end{aligned} \tag{19}$$

$$\frac{\partial}{\partial t}\bar{D}^{<}(t,t') = \sum_{\sigma}\int_{-\infty}^{t'} \mathrm{d}\bar{t}\,\bar{K}^{<}_{\varepsilon_U}(t,\bar{t})\bar{P}^{<}_{-\sigma}(t,\bar{t})\left[\bar{D}^{\mathrm{R}}(t',\bar{t})\right]^{*} - \sum_{\sigma}\int_{-\infty}^{t} \mathrm{d}\bar{t}\,\bar{K}^{>}_{\varepsilon_U}(t,\bar{t})\bar{P}^{\mathrm{R}}_{-\sigma}(t,\bar{t})\bar{D}^{<}(\bar{t},t') \tag{20}$$

with

$$\bar{K}^{\gtrless}_{\varepsilon}(t,t') = \sqrt{\Gamma_{\varepsilon(t)}(t)\Gamma_{\varepsilon(t')}(t')}\,\bar{f}^{\gtrless}_{\varepsilon}(t,t') \tag{21}$$

and

$$\bar{f}^{\gtrless}_{\varepsilon}(t,t') = \exp\left[+\mathrm{i}\int_{t'}^{t}\mathrm{d}\bar{t}\,\varepsilon(\bar{t})\right] f^{\gtrless}(t-t'), \tag{22}$$

where $f^{<}(t) = 1 - f^{>}(t)$ is the Fourier transform of the Fermi function $f^{<}(\varepsilon)$ defined by

$$f^{<}(t) = \int\frac{\mathrm{d}\varepsilon}{2\pi} f^{<}(\varepsilon)\exp\left[-\mathrm{i}\varepsilon t\right]. \tag{23}$$

The function $\bar{K}^{\gtrless}_{\varepsilon}(t,t')$, which contains the temperature dependence, entails an approximate momentum summation. From the diagrams shown in figure 4 one initially obtains

$$K^{\gtrless}(t,t') = \int\frac{\mathrm{d}\varepsilon}{2\pi}\sqrt{\Gamma_{\varepsilon}(t)\Gamma_{\varepsilon}(t')}f^{\gtrless}(\varepsilon) \times \exp\left[-\mathrm{i}\varepsilon(t-t')\right] \tag{24}$$

with an energy integration extending over the range of the conduction band and $\Gamma_{\varepsilon}(t)$ given by equation (10) with $\varepsilon(t)$ replaced by the integration variable ε. To avoid the numerically costly energy integration Nordlander and co-workers employed two different approximations: in [22] they replaced $\Gamma_{\varepsilon}(t)$ by an average over the energy range of the conduction band while in [23] they replaced it by $\Gamma_{\varepsilon(t)}(t)$ with $\varepsilon(t)$ set to $\varepsilon_0(t)$ or $\varepsilon_U(t)$ depending on which state is considered in the hybridization self-energy. Using the latter leads to

$$K^{\gtrless}_{\varepsilon}(t,t') \simeq \sqrt{\Gamma_{\varepsilon(t)}(t)\Gamma_{\varepsilon(t')}(t')}\,f^{\gtrless}(t-t') \tag{25}$$

and eventually to $\bar{K}^{\gtrless}_{\varepsilon}(t,t')$ as given in equation (21). The subscript ε indicates now not an integration variable but the functional dependence on $\varepsilon(t)$. We employ this form but keep in mind that it is an approximation to the non-crossing self-energies.

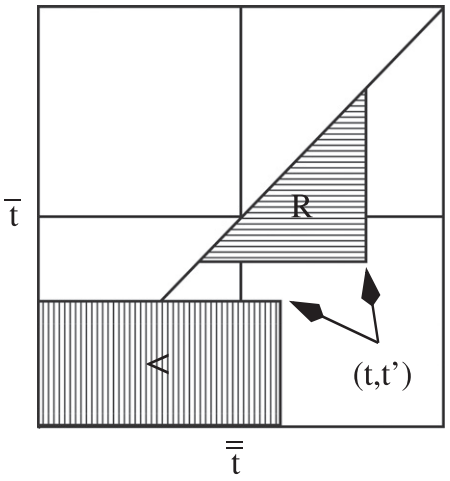

Figure 5. Sketch of the domains in the $(\bar{t}, \bar{\bar{t}})$ plane over which equations (15)–(20) have to be integrated subject to the boundary conditions (30)–(33), respectively, in order to determine the retarded and less-than Green functions at (t, t'). The triangular (rectangular) region denotes the domain required for the calculation of the retarded (less-than) Green functions.

The instantaneous (pseudo) occurrence probabilities for the projectile configurations AE^{2+}, AE^{+}, and AE^{0} are then given by

$$n_e(t) = \bar{E}^{<}(t,t), \tag{26}$$

$$\tilde{n}_{\sigma}(t) = \bar{P}^{<}_{\sigma}(t,t), \tag{27}$$

$$n_d(t) = \bar{D}^{<}(t,t), \tag{28}$$

respectively, where we refer to all of them as (pseudo) occurrence probabilities also strictly speaking n_d and n_e are true ones and only $\tilde{n}_{\sigma}$ is a pseudo occurrence probability in the sense that the true probability with which the AE^{+} configuration occurs is $n_{\sigma} = \tilde{n}_{\sigma} + n_d$ [23]. Sometimes we will also refer to n_e, $\tilde{n}_{\sigma}$, and n_d simply as (pseudo) occupancies. For the AE ion the probability for neutralization at the surface (wall recombination) is the probability for double occupancy after the completion of the trajectory, that is

$$\alpha_w = n_d(\infty), \tag{29}$$

subject to the initial conditions $n_d(-\infty) = n_e(-\infty) = 0$ and $\tilde{n}_{\sigma}(-\infty) = \delta_{\sigma,1/2}$.

We solve the two coupled sets of integro-differential equations (15)–(17) and (18)–(20) on a two-dimensional time grid setting

$$\bar{E}^{\mathrm{R}}(t,t) = \bar{P}^{\mathrm{R}}_{\sigma}(t,t) = \bar{D}^{\mathrm{R}}(t,t) = 1 \tag{30}$$

for the retarded Green functions and

$$E^{<}(-\infty,-\infty) = n_e(-\infty) = 0, \tag{31}$$

$$P^{<}_{\sigma}(-\infty,-\infty) = \tilde{n}_{\sigma}(-\infty) = \delta_{\sigma,1/2}, \tag{32}$$

$$D^{<}(-\infty,-\infty) = n_d(-\infty) = 0 \tag{33}$$

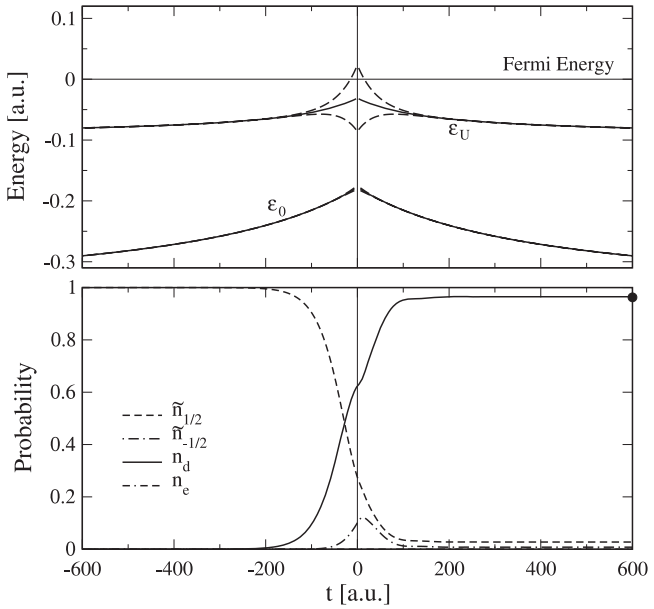

Figure 6. Upper panel: energy level diagram for the Mg:Au system at $T_s = 400$ K as a function of time. The projectile starts at $t = -600$ and $z = z_{\max} = 20$ with velocity $v = 0.024$, reaches at $t = 0$ the turning point $z = z_0 = 5$, and approaches at $t = 600$ again $z_{\max}$. The ionization levels (solid lines) are broadened according to $\epsilon_{0,U} \pm \Gamma_{0,U}$ (dashed lines) with $\Gamma_{0,U}$ as shown in figure 2. Lower panel: instantaneous (pseudo) occurrence probabilities along the trajectory for the Mg^+, the Mg^0, and the Mg^{2+} configurations. Initially, at time $t = -600$, the projectile is in the Mg^+ configuration. The neutralization probability in this particular case is $\alpha_w = n_d(600) = 0.965$ (solid bullet).

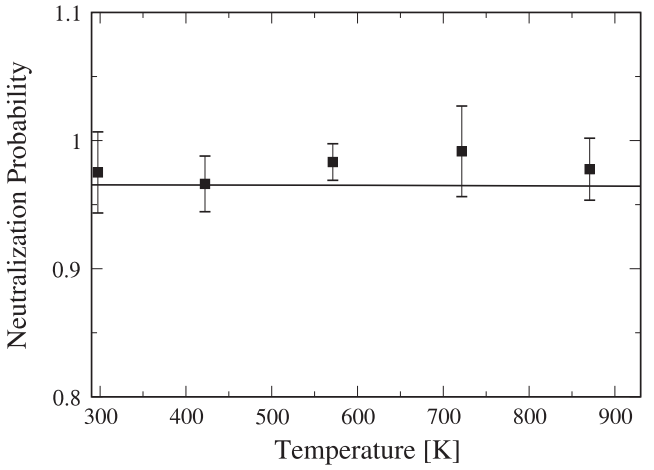

Figure 7. Temperature dependence of the neutralization probability $\alpha_w = n_d(\infty)$ for a Mg^+ ion hitting with $v = 0.024$ a gold surface. The turning point $z_0 = 5$. Also shown are experimental data from [19].

for the less-than Green functions using basically the same numerical strategy as Shao and coworkers [22, 23].

Due to the intertwining of the time integrations the integration domains for the retarded Green functions are triangular whereas for the less-than Green function they are rectangular as shown in figure 5. The size of the time-grid as well as the discretization depend on the velocity of the projectile and the maximum distance it has from the surface. For the He–Yarmoff experiment the velocities are on the order of 0.01 in atomic units. The maximum distance from which the ion starts its journey can be taken to be 20 Bohr radii. At this distance the coupling between the surface and the ion is vanishingly small. We empirically found the algorithm to converge for a $N \times N$ grid with $N = 1000$–3000. Since the Green functions are complex the computations are time and memory consuming.

4. Results

We now analyze the He–Yarmoff experiment [18, 19] quantitatively from a many-body theoretical point of view. For that purpose we combine the model developed in section 2 with the quantum-kinetics described in section 3. Besides the parameters given in table 1 we also need the velocity of the projectile. In general, the velocity will be different on the in- and outgoing branch of the trajectory. The outgoing branch, however, determines the final charge state of the projectile. We take therefore—for both branches—the normal component of the experimentally measured post-collision velocity. If not noted otherwise all quantities are in atomic units, that is, energies are measured in Hartrees and lengths in Bohr radii.

First, we discuss the Mg:Au system. In figure 6 we show the time-dependence of the broadened ionization levels, ε_U and ε_0, together with the instantaneous (pseudo) occurrence probabilities $\tilde{n}_{\pm}1/2$, n_d, and n_e for the Mg^+, the Mg^0, and the Mg^{2+} configuration, respectively. Negative and positive times denote the in- and outcoming branch of the trajectory. The velocity $v = 0.024$ and the surface temperature $T_s = 400$ K. Initially, the projectile is in the Mg^+ configuration, that is, the lower level ε_0, representing single occupancy, is occupied while the upper level ε_U, representing double occupancy, and thus the Mg^0 configuration, is empty. While the projectile is on its way through the trajectory the ionization levels shift and broaden. As a result the occupancies change. The neutralization probability is then the probability for double occupancy at the end of the trajectory.

For the particular case of the Mg:Au system the first ionization level, ε_U, that is, the level which has to accept an electron in order to neutralize the ion, is below the Fermi energy of the metal throughout the whole trajectory. The broadening is also rather weak. It only leaks for a very short time span above the Fermi energy. As a result, the magnesium ion can efficiently soak in a second electron while the electron already present due to the initial condition is basically frozen in the second ionization level. The electron captured from the metal has moreover a strong tendency to stay on the projectile. It only has a chance to leave it in the short time span where the instantaneous broadening $\Gamma_U(t)$ is larger than $|E_F - \varepsilon_U(t)|$. The neutralization probability is thus expected to be close to unity. Indeed, we find for the situation shown in figure 6 $\alpha_w = n_d(\infty) = 0.965$ (solid bullet in figure 6).

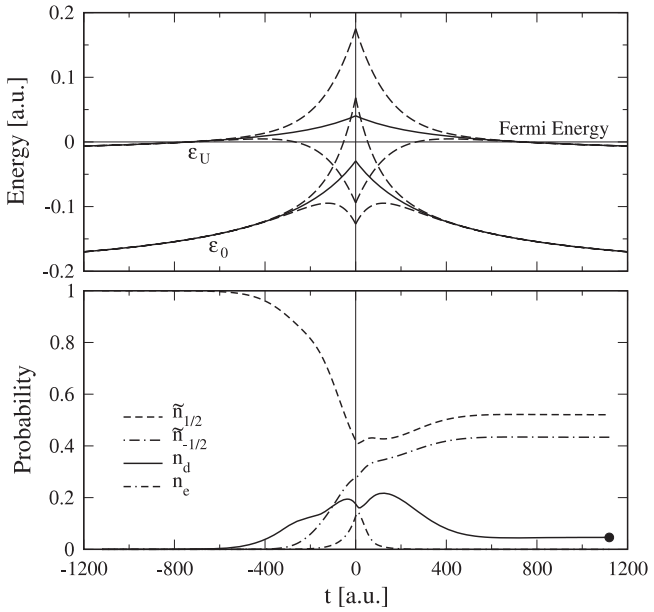

Figure 8. Upper panel: energy level diagram for the Sr:Au system at $T_s = 400$ K as a function of time. The projectile starts at $t = -1120$ and $z = z_{\max} = 20$ with velocity $v = 0.0134$, reaches at $t = 0$ the turning point $z = z_0 = 5$, and approaches at $t = 1120$ again $z = z_{\max}$. The levels (solid lines) are broadened according to $\epsilon_{0,U} \pm \Gamma_{0,U}$ (dashed lines) with $\Gamma_{0,U}$ as shown in figure 2. Lower panel: instantaneous (pseudo) occurrence probabilities along the trajectory for the Sr^+, the Sr^0, and the Sr^{2+} configurations. Initially, at time $t = -1120$, the projectile is in the Sr^+ configuration. The neutralization probability in this particular case is $\alpha_w = n_d(1120) = 0.046$ (solid bullet).

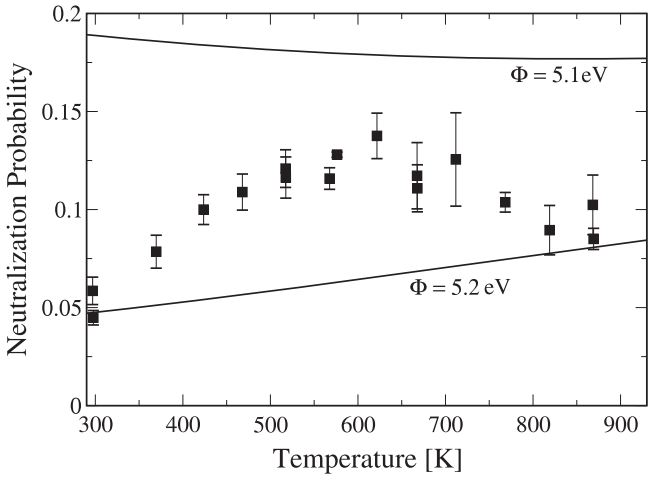

Figure 9. Temperature dependence of the neutralization probability $\alpha_w = n_d(\infty)$ for a Sr^+ ion hitting with $v = 0.0134$ a gold surface. The turning point $z_0 = 5$. Also shown are experimental data from [19].

The temperature dependence of α_w is shown in figure 7. In accordance with experiment we find α_w essentially to be independent of temperature. This is expected because both ionization levels, ε_U and ε_0, are below the Fermi energy and their broadening is too small to allow a charge-transfer from the projectile to empty conduction band states of the surface. Notice, the excellent agreement between theory and experiment indicating that the semi-empirical model we developed in section 2 captures the essential features of the charge-transfer pretty well.

After the successful description of the Mg:Au system let us now turn to the Sr:Au system. In figure 8 we again plot as a function of time the broadened ionization levels and the (pseudo) occurrence probabilities for the three configurations of the projectile. As it was the case for Mg:Au, the configuration of the projectile, which initially was in the configuration representing single occupancy, changes along the trajectory. The changes are however more subtle.

The reason is the level structure. In contrast to the Mg:Au system, the ionization levels are now closer to the Fermi energy of the surface. The first ionization level ε_U even crosses the Fermi energy with far reaching consequences. The part of the trajectory where ε_U is below the Fermi energy, that is, the region where the neutral atom would be energetically favored, the broadening is very small, indicating negligible charge-transfer from the metal to the ion and hence a stabilization of the ion due to lack of coupling. When the broadening and thus the coupling is large ε_U is above the Fermi level. In this part of the trajectory the ion is energetically stabilized. The first ionization level of strontium can capture an electron from the metal only in the time span where $|E_F - \varepsilon_U(t)| < \Gamma_U(t)$. The neutralization probability of a strontium ion should be thus much smaller than the one for a magnesium ion. Indeed we find $\alpha_w = n_d(\infty) = 0.046$ which is much smaller than unity (solid bullet in figure 8).

Due to the shift and broadening of the first ionization level ε_U it is clear that a strontium ion cannot as efficiently neutralize on a gold surface as a magnesium ion. This sets the scale of α_w. In addition, and in great contrast to magnesium, the second ionization level ε_0 is however also close to the Fermi energy. In those parts of the trajectory for which $|E_F - \varepsilon_0(t)| < \Gamma_0(t)$ it can affect the charge-transfer between the metal and the projectile. In fact, taken by itself, it should stabilize the ion and hence decrease the neutralization probability [12]. Qualitatively, this can be understood from a density of states argument. From the upper panel of figure 8 we can infer that the broadened second ionization level is cut by the Fermi energy in the upper half of its local density of states. Hence, close to the surface holes start to occupy the second ionization level at energies where the local density of states is higher than at the energies where electrons are transferred. Increasing temperature enhances thus the tendency of electron loss from the second ionization level. Without interference from the first ionization level the neutralization probability should thus go down with temperature.

That the second ionization level of Sr comes close to the Fermi energy of Au most probably led He and Yarmoff [18, 19] to suggest that the neutralization of strontium ions on gold surfaces is dominated by electron correlations. Indeed the experimentally found negative temperature dependence of α_w above $T_s = 600$ K seems to support their conclusion. However, the temperature dependence of α_w we obtain and

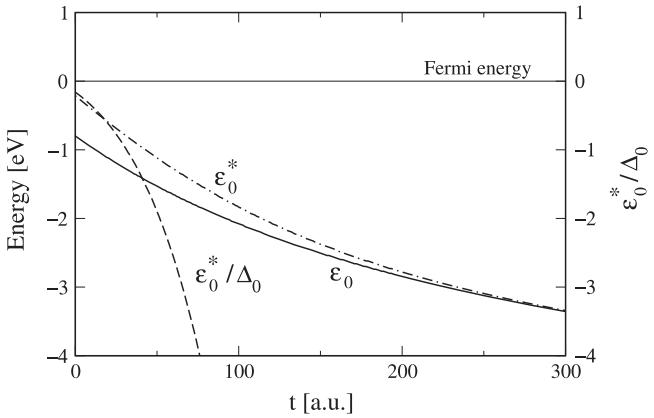

Figure 10. Renormalized (ε_0^*) and bare (ε_0) second ionization level measured from the Fermi energy as a function of time traveled along the outgoing branch of the trajectory for the Sr:Au system with $v = 0.0134$ and $T_s = 400$ K. Also shown as a function of time is the scaling invariant ε_0^*/Δ_0. In the region for which $|\varepsilon_0^*/\Delta_0| < 1$ the system is likely to be in the mixed-valence region. The material parameters are as given in table 1 and $v = 0.0134$.

which we plot in figure 9, does not show this behavior, at least, for the material parameters of table 1 and the experimentally measured post-collision velocity. The reason for the discrepancy between the measured and the calculated data is unclear. The material parameters seem to be reasonable since the theoretical results have the correct order of magnitude. It could be however that the temperature-induced transfer of holes to the second ionization level is overcompensated by the electron-transfer to the first ionization level. In the region where charge-transfer is strongest the two ionization levels overlap. The absence of energy separation together with the conditional temporal weighting due to the dynamics of the collision process makes it very hard to tell *a priori* which process will win and manifest itself in the measured neutralization probability.

So far, the discussion of the data left out the possibility of a correlation-induced sharp resonance in the vicinity of the Fermi energy, that is, the key feature of Kondo-type physics. The numerical results seem to suggest that either there is no resonance or it does not affect the neutralization process. However, from the data itself we cannot determine which one is the case. We can thus not decide whether the Sr:Au system is in a correlated regime or not and hence whether an interpretation of the experimental data in terms of a mixed-valence scenario is in principle plausible or has to be dismissed. A rigorous way to decide this would be to calculate the instantaneous spectral functions for the projectile and to look for sharp resonances in the vicinity of the Fermi energy. This is beyond the scope of the present work.

To get at least a qualitative idea about in what regime the strontium projectile might be along its trajectory we plot in figure 10, following Merino and Marston, [12] Haldane's scaling invariant, [45]

$$\frac{\varepsilon_0^*}{\Delta_0} = \varepsilon_0 + \frac{\Delta_0}{\pi}\log\left(\frac{U}{\Delta_0}\right), \tag{34}$$

as a function of time travelled along the outgoing branch of the trajectory. In the perturbative regime which is strictly applicable only far away from the surface ε_0^* can be interpreted as the renormalized second ionization level and $\Delta_0 = \Gamma_0/2$ [23]. For $|\varepsilon_0^*/\Delta_0| < 1$ the projectile is likely to be in the mixed-valence regime [12]. Since ε_0^* comes very close to the Fermi energy holes are expected to transfer in the mixed-valence regime very efficiently to the projectile. In situations where the projectile stays sufficiently long in the mixed-valence regime before ε_0^* crosses the Fermi energy double occupancy and hence the neutralization probability should be suppressed with increasing temperature.

As can be seen in figure 10 close enough to the surface the strontium projectile is indeed in the mixed-valence regime. For the material parameters given in table 1 and the experimental value for the projectile velocity the time-span however is rather short. Most probably this is the reason why we do not see any reduction of α_w with temperature for the parameters we think to be best suited for the Sr:Au system. Since the experimental data are unambiguous, this indicates perhaps the need for a precise first-principle calculation of the model parameters. Alternative interpretations of the experimental results can however not be ruled out.

5. Conclusions

Motivated by claims that the neutralization of strontium ions on gold surfaces is affected by electron correlations we set up a semi-empirical model for charge-transferring collisions between AE projectiles and noble metal surfaces. The surface is simply modelled by a step potential while the projectile is modelled by its two highest ionization levels which couple to the surface via Gadzuk's image-potential-based projectile-surface interaction. To calculate the neutralization probability we employed a pseudo-particle representation of the projectile's charge states and quantum-kinetic equations for the retarded and less-than Green functions of the projectile as initially suggested by Nordlander, Shao and Langreth. Besides the non-crossing approximation for the self-energies and an approximate momentum summation no further approximations are made. The quantum-kinetic equations are numerically solved on a two-dimensional time-grid using essentially the same strategy as Shao and coworkers.

The absolute values for the neutralization probability we obtain are in good agreement with experimental data, especially for the Mg:Au system, but also for the Sr:Au system, although for the latter we could not reproduce the temperature dependence of the neutralization probability. Our calculations can thus not decide whether the He–Yarmoff experiment can be interpreted in terms of a mixed-valence scenario. From the instantaneous values of Haldane's scaling invariant we see however that the Sr:Au system could be in the mixed-valence regime. The mechanism for a negative temperature dependence, that is, the possibility of efficiently transferring holes to the second ionization level, is thus in principle present. For the material parameters however most appropriate for Sr:Au

the negative temperature dependence arising from this channel seems to be overcompensated by the positive temperature dependence of the electron-transfer to the first ionization level. To prove that He and Yarmoff have indeed seen—for the first time—mixed-valence correlations affecting charge-transfer between an ion and a surface requires therefore further theoretical work.

Acknowledgments

MP was funded by the federal state of Mecklenburg-Western Pomerania through a postgraduate scholarship within the International Helmholtz Graduate School for Plasma Physics. In addition, support from the Deutsche Forschungsgemeinschaft through project B10 of the Transregional Collaborative Research Center SFB/TRR24 is greatly acknowledged.

References

[1] Winter H-P and Burgdörfer J (ed) 2007 *Slow Heavy-Particle Induced Electron Emission From Solid Surface* (Berlin: Springer)
[2] Rabalais J W (ed) 1994 *Low Energy ion–surface Interaction* (New York: Wiley)
[3] Los J and Geerlings J J C 1990 *Phys. Rep.* **190** 133
[4] Brako R and Newns D M 1989 *Rep. Prog. Phys.* **52** 655
[5] Modinos A 1987 *Prog. Surf. Sci.* **26** 19
[6] Yoshimori A and Makoshi K 1986 *Prog. Surf. Sci.* **21** 251
[7] Czanderna A W and Hercules D M 1991 *Ion Spectroscopies for Surface Analysis* (New York: Plenum)
[8] Harada Y, Masuda S and Ozaki H 1997 *Chem. Rev.* **97** 1897
[9] Kraus W, Falter H-D, Fantz U, Franzen P, Heinemann B, McNeely P, Riedl R and Speth E 2008 *Rev. Sci. Instrum.* **79** 02C108
[10] Lieberman M A and Lichtenberg A J 2005 *Principles of Plasma Discharges and Materials Processing* (New York: Wiley)
[11] Shao H, Langreth D C and Nordlander P 1996 *Phys. Rev. Lett.* **77** 948
[12] Merino J and Marston J B 1998 *Phys. Rev.* B **58** 6982
[13] Hewson A C (ed) 1993 *The Kondo Problem to Heavy Fermions* (Cambridge: Cambridge University Press)
[14] Grabert H and Devoret M H (ed) 1992 *Single Charge Tunneling: Coulomb Blockade Phenomena in Nanostructures* (New York: Plenum)
[15] Wingreen N S and Meir Y 1994 *Phys. Rev.* B **49** 11040
[16] Aguado R and Langreth D C 2003 *Phys. Rev.* B **67** 245307
[17] Ternes M, Heinrich A J and Schneider W-D 2009 *J. Phys.: Condens. Matter* **21** 1
[18] He X and Yarmoff J A 2010 *Phys. Rev. Lett.* **105** 176806
[19] He X and Yarmoff J A 2011 *Nucl. Instrum. Meth. Phys. Res.* B **269** 1195
[20] Langreth D C and Nordlander P 1991 *Phys. Rev.* B **43** 2541
[21] Nordlander P, Shao H and Langreth D C 1993 *Nucl. Instrum. Meth. Phys. Res.* B **78** 11
[22] Shao H, Langreth D C and Nordlander P 1994 *Phys. Rev.* B **49** 13929
[23] Shao H, Langreth D C and Nordlander P 1994 *Low Energy Ion–surface Interaction* ed J W Rabalais (New York: Wiley) p 117
[24] Kasai H and Okiji A 1987 *Surf. Sci.* **183** 147
[25] Nakanishi H, Kasai H and Okiji A 1988 *Surf. Sci.* **197** 515
[26] Romero M A, Flores F and Goldberg E C 2009 *Phys. Rev.* B **80** 235427
[27] Bajales N, Ferrón J and Goldberg E C 2007 *Phys. Rev.* B **76** 245431
[28] Goldberg E C, Flores F and Monreal R C 2005 *Phys. Rev.* B **71** 035112
[29] Onufriev A V and Marston J B 1996 *Phys. Rev.* B **53** 13340
[30] Marston J B, Andersson D R, Behringer E R, Cooper B H, DiRubio C A, Kimmel G A and Richardson C 1993 *Phys. Rev.* B **48** 7809
[31] Gadzuk J W 1967a *Surf. Sci.* **6** 133
[32] Gadzuk J W 1967b *Surf. Sci.* **6** 159
[33] Clementi E and Roetti C 1974 *At. Data Nucl. Data Tables* **14** 177
[34] Coleman P 1984 *Phys. Rev.* B **29** 3035
[35] Kotliar G and Ruckenstein A E 1986 *Phys. Rev. Lett.* **57** 1362
[36] Kadanoff L P and Baym G 1962 *Quantum Statistical Mechanics* (New York: Benjamin)
[37] Keldysh L V 1965 *Sov. Phys.—JETP* **20** 1018
Keldysh L V 1964 *J. Exp. Theor. Phys. (USSR)* **47** 1515 (in Russian)
[38] Nordlander P and Tully J C 1990 *Phys. Rev.* B **42** 5564
[39] Marbach J, Bronold F X and Fehske H 2011 *Phys. Rev.* B **84** 085443
[40] Marbach J, Bronold F X and Fehske H 2012 *Eur. Phys. J.* D **66** 106
[41] Marbach J, Bronold F X and Fehske H 2012 *Phys. Rev.* B **86** 115417
[42] Newns D M, Makoshi K, Brako R and van Wunnik J N M 1983 *Phys. Scr.* **T6** 5
[43] Slater J C 1930 *Phys. Rev.* **36** 57
[44] Langreth D C and Wilkins J W 1972 *Phys. Rev.* B **6** 3189
[45] Haldane F D M 1978 *Phys. Rev. Lett.* **40** 416